Mapping vineyard foliage density with multispectral proxidetection imagery

Marie-Aure Bourgeon, Jean-Noël Paoli, Gawain Jones, Sylvain Villette, Christelle Gée

Mapping vineyard folliage density with multispectral proxidection imagery

Bourgeon M-A., Paoli J-N., Gée C., Jones G., Villette, S.
UMR 1347Agroécologie, EcolDur Dept., Precision Agriculture Team,
AgroSup Dijon
BP 87999- 21079 Dijon
jn.paoli@agrosupdijon.fr

***Abstract*— In Precision Viticulture, imaging systems are increasingly used for the characterization of vines in order to develop new approaches to vineyard management. Most of them are based on remote sensing. This paper presents a new multispectral imaging system and a new approach to map vineyard leaf development. It is based on the use of a 2-CCD camera, the first one is a RGB sensor and the second one a NIR sensor. This camera is embedded on a track laying tractor and associated with a GNSS system. It works with natural ambient light. A Greenseeker is also embedded to validate the first results of imagery. It is a sensor usually used in viticulture to assess the foliage density of vines.**

The images are calibrated in order to correct geometric distortion and variations of the natural light. The parameters of the geometric correction are stable over time, whereas the radiometric correction needs to include a color checker in the background of all the images. For each of them, a calibration model is computed and reflectance of objects is obtained. The calibrated images can be compared with each other.

During 2013, four datasets of about 5000 images were acquired. For all the images, a vegetation index is performed to retrieve agronomic information. Based on these images, different vineyard maps were generated with calibrated images, with non-calibrated images, and with Greenseeker values. We present and discuss some of them in order to assess the relevancy of the approach.

Keywords— calibration, multispectral imagery, proxidetection, vine folliage, precision viticulture, agroecology

I. INTRODUCTION

Precision viticulture is the application of Precision Agriculture to the vine-growing context [1, 2]. The approach is based on the same steps: observation, characterization, recommendations, application, georeferencing data. It aims to account for infield variability and to optimize vineyard management [1, 3, 4, 5].

In recent years, imaging systems are increasingly used for the observation step [3]. Many of them are based on remote sensing from aerial to satellite imagery (ie. Oenoview). More recently, new applications using infield diagnostic tools have been developed in order to estimate yield or quality of grapes [6, 7, 8], detection of diseases [9, 10] and phenology [11, 12]. A complete review of this tools has been proposed by Whalley [13].

This paper presents a new proximity imaging tool to study vine foliage. First, it describes the experimental site and the acquisition system, which consists in the association of a GNSS (Global Navigation Satellite System) and a multispectral camera (red (R), green (G), blue (B), near infrared (NIR)), embedded on a track laying tractor. Second, it details the post-treatment algorithms and the agronomic indexes computed from the images. Third it presents first results of the approach. It shows maps of agronomic indexes provided by our approach and discusses their relevancy.

The main part of this this work deals with the post-treatment of the image, which associates a geometric and a radiometric calibration. The geometric calibration aims to correct the distortion caused by the optical system. The radiometric calibration is needed to compute reflectance values from luminance values acquired in natural light. It allows to compute agronomic indexes such as NDVI (Normalized Difference Vegetation Index), which characterizes the foliage density of the vines.

II. MATERIAL

A. Experimental vineyard

The experiments are conducted in an experimental site of wine technical institute named "CIVC (Comité interprofessionnel du Vin de Champagne)". It is based near Epernay, in the region of Champagne (North-Est of France).

The test plot has an area of 0.72 Ha. It was planted in 1996 with a high density. The inter-row distance is 110 cm, the distance between stocks is 120 cm, and the height of trimming is 127 cm.

Many experiments were conducted at this plot since planting in order to understand which parameters influence vines development. The technical institute has an historical background and traceability for many agronomic, climatic, and physiological parameters.

The plot has been divided in three areas (low, medium, and high), and three grape varieties were planted on each area: Black Pinot (PN), Chardonnay (CH), and Meunier (Mn). So, nine

blocks have been delineated and planting followed a Latin-Square design. The blocks are described Figure 1.

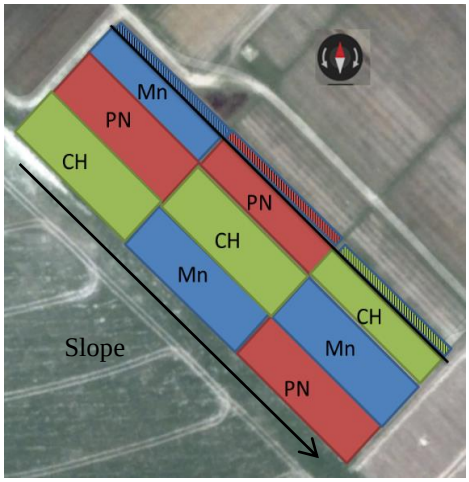

Fig. 1. Blocks delineated in the experimental vineyard (PN: black pinot, CH: Chardonnay, Mn: Meunier)

B. Multispectral imaging system

A multispectral camera has been embedded on a track laying tractor which can move between vine rows. When acquiring images, its speed is between 2 and 4 km/h, depending on field conditions (tillage, slope...). It is located by a centimetric-level global positioning system (GPS) in order to allow a spatio-temporal analysis of the information gathered by the camera. A Greenseeker sensor has also been embedded. It is an active sensor commonly used in agriculture and viticulture. It acquires data in two wavelengths (red and near infrared) and computes a vegetation index named NDVI (Normalized Difference Vegetation Index).

Camera, Greenseeker, and GPS are controlled by a laptop. A black panel is also carried by the tractor. It takes place behind leaf hedge and serves as background for data acquisition. Figure 2 shows the tractor and the acquisition system.

The multispectral camera is JAI's AD-130GE. It is a prism-based 2-CCD camera capable of simultaneously capturing visible and near-infrared rays through the same optical path using two individual channels. The first channel has a Bayer mosaic color sensor that captures visible light, while the second channel has a monochrome sensor for capturing near infrared light. It is designed around Sony's ICX447 CCD series (1296 x 966 pixels) for 1.3 megapixels of resolution per channel.

The short distance between camera and leaf hedge requires a wide angle lens. We chose a focal length of 2.8 mm. It provides images which represent an average field of view of 90 cm by 67 cm. The configuration of the optical system is described in Figure 2. An example image of RGB and IR is displayed Figure 3. The tractor speed is around 1 m/s and the camera acquires 3 images per second. Each image describes one vine stock.

Aperture and exposure time are fixed by the operator before each dataset acquisition. Aperture is chosen according to ambient light. Exposure time is set in order to avoid blurred image. Sensor's gain is controlled in real time by the laptop and it is adjusted in case of underexposure or overexposure.

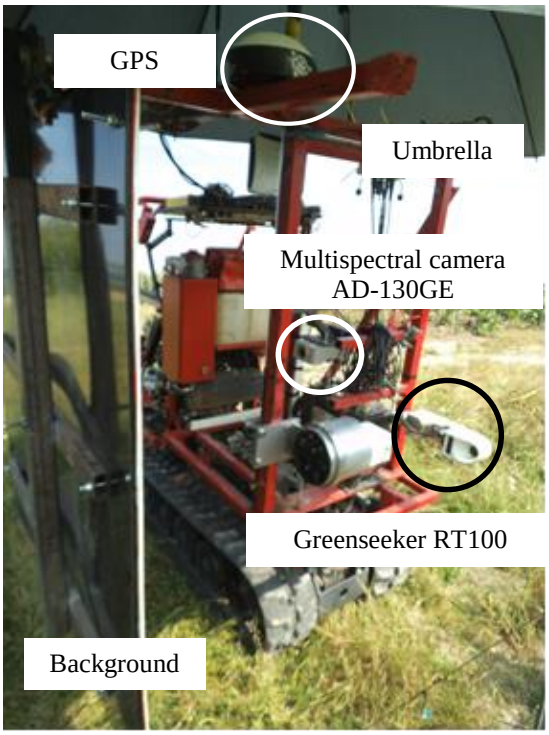

Fig. 2. The multispectral camera, Greenseeker and the GPS embedded on the track laying tractor

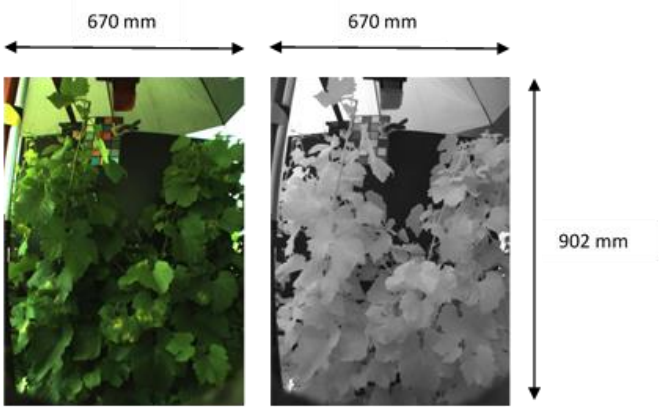

Fig. 3. Sample RGB image provided by the multispectral camera

C. Sampling plan

The plot contains 45 rows. One over two rows is used for image acquisition. For each studied row, images of all the stocks were registered. Four datasets were obtained in 2013 in this experimental vineyard and the Table I summarizes their characteristics.

TABLE I. DATES OF ACQUISITIONS AND NUMBER OF IMAGES ACQUIRED IN THE EXPERIMENTAL VINEYARD

Dataset	N°1	N°2	N°3	N°4
Date	17/07/14	13/08/14	27/08/14	24/09/14
Hour	11h-12h	14h-15h	15h-16h	14h-15h
Number of images per dataset	5356	6556	6280	6336

III. METHOD

A. Geometric calibration of an image

A prism-based 2-CCD camera associated with a wide angle lens creates distortions in the images. These distortions are different for each sensor, according to the light path through the prism. It is necessary to correct geometric distortion in order to compute morphometric indicators (such as leaves areas).

The toolkit we use to correct geometric distortion provided by Bouget [14]. It is is based on the work of Zhang [15]. The distortion is considered to be the same on all the images acquired by a camera. This distortion can be measured on images of a known reference, which is a checkerboard of 196 squares and of 56 cm side. An algorithm can be used to correct all the images according to the information provided by images of the checkerboard.

Figure 4 presents an image of the checkerboard. Figure 4.a displays the raw image while figure 4.b displays the result of the calibration algorithm.

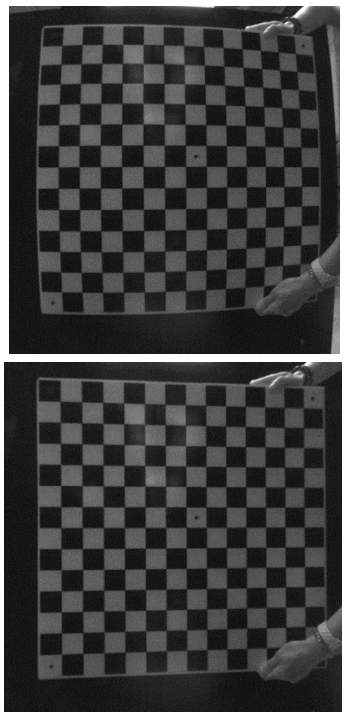

(a)

(b)

Fig. 4. Checkerboard used to perform the geometric calibration. (a) raw image provided by the camera ; (b) corrected image after calibration

B. Radiometric calibration of an image

Images are acquired in broad daylight. The intensity of the illumination and the presence of shadows cannot neither be controlled or nor be considered as stable over time. Some technical approaches have been implemented to partially control these features, such as occulting objects or light diffusing materials. At this step, illumination can be considered as homogeneous for all the pixels of an image.

However, the ambient light is not constant over all the acquired images and the luminance values of the natural objects (such as the leaves) cannot be analyzed and compared between images. Therefore, we perform a radiometric calibration in order to compute reflectance values. This process provides the spectral signatures of natural objects in the scene and allows to extract agronomic information on foliage and to compute an agronomic index (i.e. NDVI).

The radiometric image correction is performed as a post-acquisition treatment. For this, we use a MacBeth color chart, placed in the background of the image. It is a pattern of 24 color patches which can be shown Figure 5.

Only the six neutral patches are used (the black patch, the four shaded gray patches, and the white patch).

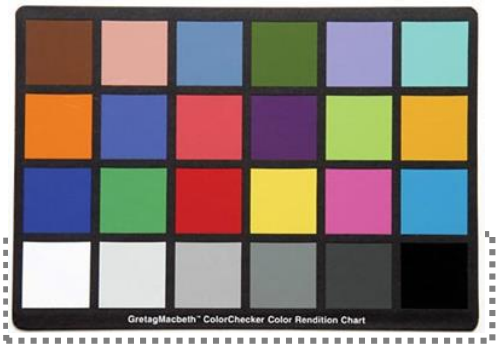

Fig. 5. MacBeth Color Char. The 6 patches used for the radiometric calibration are delineated by the dashed line.

For all of these patches, the manufacturer indicates normal luminance values in the visible range (400nm to 700nm) using standard Red Green Blue color space (sRGB). Each patch is defined by a red, a green, and a blue values, from 0 to 255.

Multispectral cameras usually use RGB color space. sRGB values result from gamma encoding. sRGB and RGB color spaces are related by formula 1.

$$\begin{aligned} sR &= R^{\gamma} \\ sG &= G^{\gamma} \\ sB &= B^{\gamma} \\ with\ \gamma &= 2.2 \end{aligned} \quad (1)$$

RGB values provided by the camera depend on reflectance ρ of the patches and on the ambient light. Standard values only depends on the reflectance ρ of the patches. The relation between reflectance values and standard values is defined by formula 2.

$$R = 255.\rho_R$$
$$G = 255.\rho_G \quad (2)$$
$$B = 255.\rho_B$$

When illumination is homogeneous for all the pixels of an image, a linear relation exists between measured and calibrated RGB values of the pixels.

Let I be an image and p be a pixel of I.

R_p, G_p, and B_p are the luminance values measured at this pixel for the red, green, and blue channels. R_p^c, G_p^c, and B_p^c are the results of the radiometric calibration.

It exist coefficients a_I and b_I for each channel such as:

$$R_p^c = a_I^R.R_p + b_I^R$$
$$G_p^c = a_I^G.G_p + b_I^G \quad (3)$$
$$B_p^c = a_I^B.B_p + b_I^B$$

The coefficients a_I (slope) and b_I (intercept) can be estimated by a linear regression between measured and normal values of the patches for each image and each channel.

In order to improve correction for RGB channels and to extend the approach to near infrared channel, reflectance values of the patches were measured, using a FieldSpec3 spectroradiometer from ASD inc. Figure 6 presents the average reflectance spectra obtained for the 6 patches. Table II presents the reflectance values selected on the spectra for each maximum waveband of the camera CCD, and the sRGB (or sNIR) values computed from them.

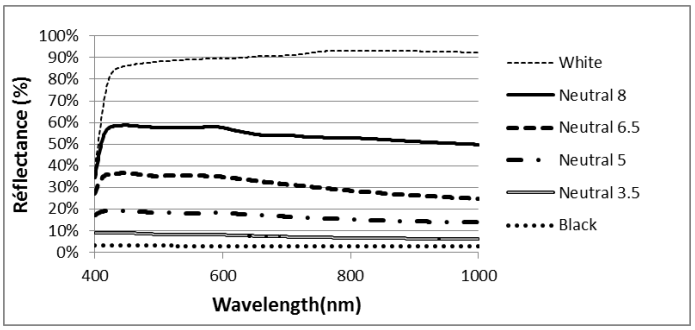

Fig. 6. The average spectra obtained for the 6 patches, using a FieldSpec 3 spectroradiometer from ASD Inc.

TABLE II. REFLECTANCE VALUES AND SRGB/SIR VALUES FOR EACH NEUTRAL PATCH

Channel		B	G	R	IR
Wavelength (nm)		450	550	600	800
White	ρ (%)	86.3%	89.1%	89.7%	93.3%
	sRGB, sNIR	220	227	229	238
Neutral 8	ρ (%)	58.7%	57.5%	57.6%	52.8%
	sRGB, sNIR	150	147	147	135
Neutral 6,5	ρ (%)	36.6%	35.4%	34.8%	28.5%
	sRGB, sNIR	93	90	89	73
Neutral 5	ρ (%)	19.2%	18.1%	18.1%	15.1%
	sRGB, sNIR	49	46	46	39
Neutral 3.5	ρ (%)	8.9%	8.2%	8.0%	6.6%
	sRGB, sNIR	23	21	20	17
Black	ρ (%)	3.1%	2.9%	2.9%	2.9%
	sRGB, sNIR	8	7	7	7

This result allows to extend to extend the relations 1, 2 and 3 to the infrared channel as following:

$$sNIR = NIR^{\gamma} \ (with\ \gamma = 2.2)$$
$$NIR = 255.r_{NIR} \quad (4)$$
$$NIR_p^c = a_I^{NIR}.NIR_p + b_I^{NIR}$$

C. Estimation of a calibration map

In some images, the MacBeth color chart is hidden by leaves and cannot be used to perform the radiometric calibration. To overcome this problem, we use a linear combination of the information contained in the previous and in the next acquired images.

Let $I(n)$ be the nth image acquired by the camera. Let $I(n-1)$ and $I(n+1)$ be the previous and next images. D^+ and D^- are respectively the distance between $I(n)$ and $I(n+1)$ and between $I(n)$ and $I(n-1)$. D^+ and D^- are computed from the locations given by the GNSS.

The coefficients $a_{I(n)}$ and $b_{I(n)}$ are estimated as follows:

$$a_{I(n)} = \frac{a_{I(n-1)}.D^- + a_{I(n+1)}.D^+}{D^- + D^+}$$
$$b_{I(n)} = \frac{b_{I(n-1)}.D^- + b_{I(n+1)}.D^+}{D^- + D^+} \quad (5)$$

D. Computation of a vegetation index

Once the calibration is complete, each image contains the "pure" internal properties of the leaves (spatial signature, morphometric parameters) and can be compared with each other. So, the calibrated images are used to compute vegetation indexes. In particular, we compute an agronomic index NDVI:

Normalized Difference Vegetation Index. Its definition is given by the following equation.

$$NDVI = \frac{IR - R}{IR + R} \quad (7)$$

First, NDVI images are built. The index is computed for each pixel of each image. Second, a mean NDVI value is computed for each image. Third, a NDVI map of the experimental field is generated.

Then, the generated maps can be compared with Greenseeker maps.

IV. Results and Discussion

This part presents the results for the first dataset (acquired on July 17, 2014).

Table III shows the coefficients of determination (r^2) between normal and experimental RGB (or NIR) values. We considered all the images where the color checker was visible (3000 images in 5356). For each channel, the table presents minimum, maximum, and mean values of the coefficient.

Mean values are greater than 0.8. This reflects a good correlation between normal and experimental values. Minimum values are also greater than 0.8, except for the blue channel. Therefore, some atypical data may exist. However, the blue channel is not taken into account for the computation of NDVI.

TABLE III. Coefficients of determination between normal and measured RGB/IR values

	R	G	B	NIR
Minimum value of r^2	0.88	0.84	0.74	0.91
Maximum value of r^2	0.99	0.99	0.99	0.99
Mean value of r^2	0.98	0.97	0.96	0.97

Figure 7 describes the linear relation between experimental and normal values for the 6 neutral color patches of the MacBeth color checker. It includes one point per patch and per channel. The coordinates of these points are given by: the mean of experimental values measured on the images (for each considered patch and channel) and the normal values given by the manufacturer. The points are associated with vertical bars. These bars describe standard deviations of experimental values for all the images of the dataset.

For each channel, a straight line shows linear regression between experimental and manufactured values: this is the radiometric calibration used for image correction. Table IV presents mean slope and mean intercept of each linear function.

TABLE IV. Mean values of slope and intercept for each spectral channel

Spectral channel	B	G	R	NIR
Slope $\hat{a} = \sum_I a_I$	2.55	1	1.19	1.15
Intercept $\hat{b} = \sum_I b_I$	8.18	27.47	36.71	30.22

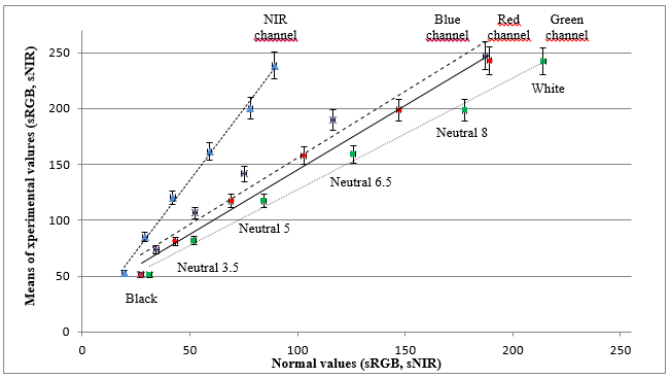

Fig. 7. Linear relation between experimental and manufactured values of the 6 neutral patches of the MacBeth Color chart.

Standard deviation increases when sRGB (or sNIR value) increases. This white patch seems being more sensitive to the variations of ambient light. This sensitivity may generate noise and the interest of using neutral 8 or white patch should be discussed in a future work.

Figure 8 shows infield variations of the coefficients a_I and b_I. These variations are important and confirm the relevancy of a radiometric calibration of each image. Some of these maps can be considered as similar.

The values of the a_I coefficients are in general rather homogeneous for all the visible channels, as the values of the b_I coefficients (maps 8a, 8b, and 8c). Conversely, the variations of the coefficients a_I and b_I computed for the near infrared channel are different from visible channel. This could be explained by the use of a 2-CCD camera. Indeed, red, green, and blue channels are acquired by the same CCD, whereas infrared values are acquired by a dedicated sensor.

For all the channels, the values of the coefficients a_I and b_I seems relatively homogeneous for a given row in a given block. This point could be studied in a complementary work.

Figure 9 presents three maps. The first one (9.a) presents infield variations of NDVI values computed with non-calibrated images, whereas the second one (9.b) presents infield variations of NDVI values computed with calibrated images. The third one is a map of the differences between the two values (expressed as a percentage of the first value). These differences can be important (up to 64 percent) and seems cover a significant area in the field. It shows the impact of the calibration step.

Figure 10 compares infield variations of NDVI values computed from multispectral images (10.a), and provided by Greenseeker (10.b). The map 10.c shows the differences between the two values (expressed as a percentage of the first value). The difference can be locally important. However, the spatial structure of the maps 10.a and 10.b are similar, and for the main part of the field, the values are close to each other. Multispectral imaging system seems being more sensitive in low values areas. Further work is needed to define sensitivity of the imaging system and to compare it with Greenseeker sensitivity.

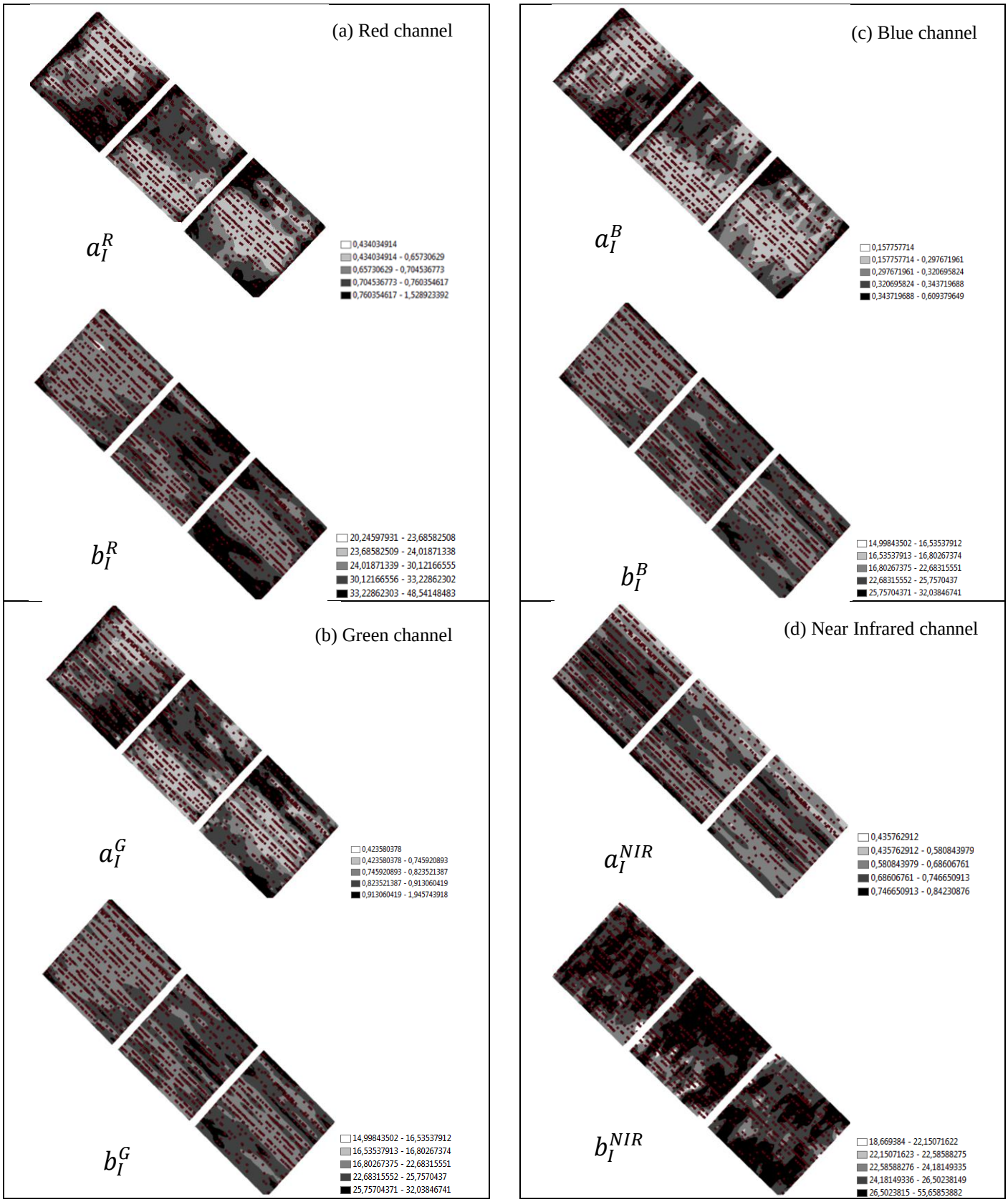

Fig. 8. Maps of a_I and b_I values for each channel. Points represents the location of acquired images

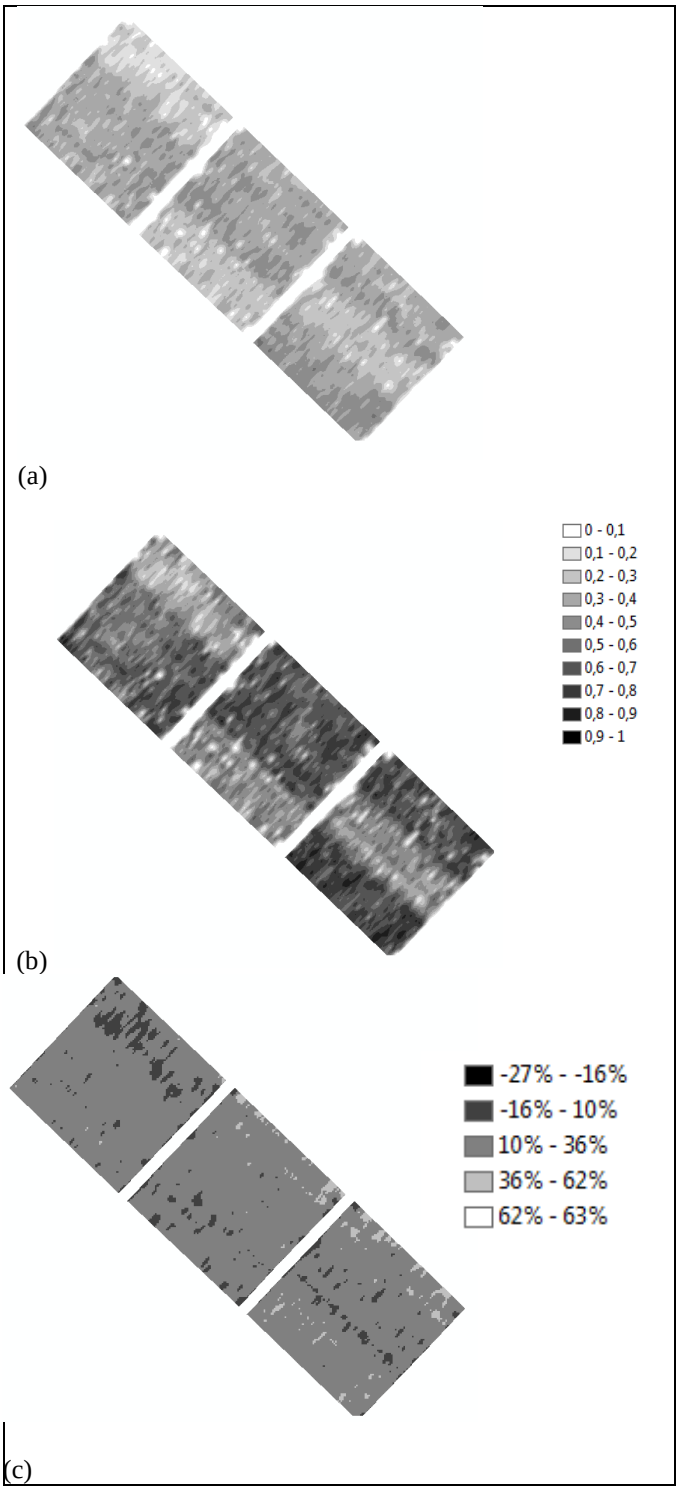

Fig. 9. (a) NDVI map obtained with non-calibrated images (b) NDVI map deduced from calibrated images (c) Map of the differences between (a) and (b)

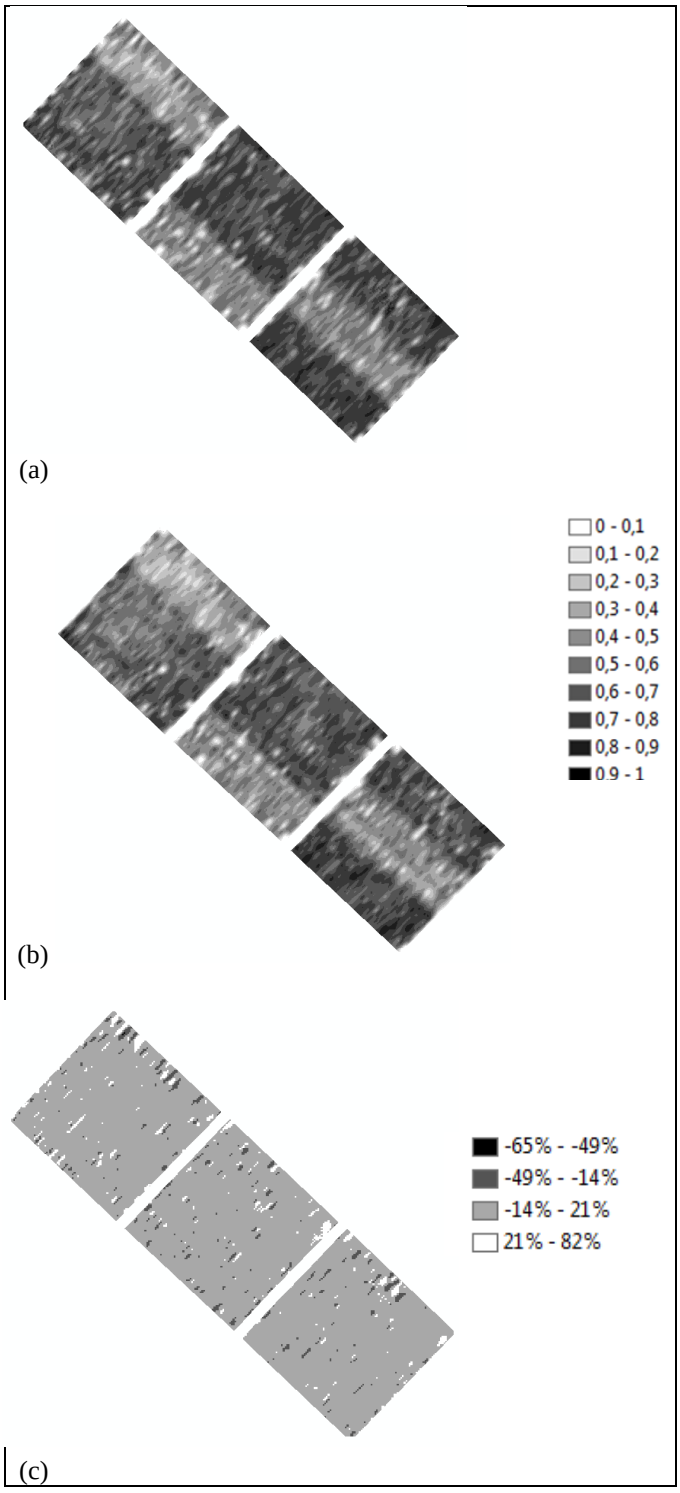

Fig. 10. NDVI map deduced from calibrated images. (b) NDVI map provided by Greenseeker data. (c) Map of the differences between (a) and (b)

V. CONCLUSION

This paper deals with a new proximity multispectral imaging system dedicated to the study of the vineyards and the characterization of the leaf hedge development. It is based on a 2-CCD camera embedded on a track laying tractor, and works with natural light. Images are post treated in order to perform a geometric and a radiometric calibration. The parameters of the geometric correction are defined for each CCD and are stable over time. The radiometric correction needs to include a color checker in the background of all the images and to compute a model of calibration for each of them.

First results are presented. Reflectance is deduced from the calibrated images, allowing to compute NDVI images, and so NDVI maps. The comparison of the maps obtained with calibrated images, with non-calibrated images, and with the Greenseeker, shows the relevancy of the image approach.

However, further work is needed in order to study the: spatial structure of the radiometric calibration parameters, to determine the optimal number of patches, to compare the sensitivity of the imaging system and the sensitivity of Greenseeker.

REFERENCES

[1] Bramley, R., & Lamb, D. (2003). Making sense of vineyard variability in Australia. Proc. Internat. Symp. on Precision ….

[2] Bramley, R., & Proffitt, A. (1999). Managing variability in viticultural production. Grapegrower and Winemaker.

[3] Bramley, R. (2001). Progress in the development of precision viticulture - variation in yield, quality and soil properties in constating australian vineyards. The Australian Grapegrower and Winemaker.

[4] Mathews, A. J. (2013). Applying Geospatial Tools and Techniques to Viticulture. Geography Compass, 7(1), 22–34. doi:10.1111/gec3.1201

[5] Tisseyre, B. (2012). Peut-on appliquer le concept d'agriculture de précison a la viticulture. Mémoire d'habilitation à diriger des Recherches.

[6] Chamelat, R., Rosso, E., Choksuriwong, A., Rosenberger, C., Laurent, H., & Bro, P. (2006). Grape Detection By Image Processing. In IECON 2006 - 32nd Annual Conference on IEEE Industrial Electronics (pp. 3697–3702). IEEE. doi:10.1109/IECON.2006.347704

[7] Dunn, G. M., & Martin, S. R. (2008). Yield prediction from digital image analysis: A technique with potential for vineyard assessments prior to harvest. Australian Journal of Grape and Wine Research, 10(3), 196–198. doi:10.1111/j.1755-0238.2004.tb00022.x

[8] Murillo-Bracamontes, E. A., Martinez-Rosas, M. E., Miranda-Velasco, M. M., Martinez-Reyes, H. L., Martinez-Sandoval, J. R., & Cervantes-de-Avila, H. (2012). Implementation of Hough transform for fruit image segmentation. Procedia Engineering, 35, 230–239. doi:10.1016/j.proeng.2012.04.185

[9] Guanlin Li, Z. M. (2011). Image Recognition of Grape Downy Mildew and Grape Powdery Mildew Based on Support Vector Machine. (pp. 151 – 162).

[10] Peressotti, E., Duchêne, E., Merdinoglu, D., & Mestre, P. (2011). A semi-automatic non-destructive method to quantify grapevine downy mildew sporulation. Journal of Microbiological Methods, 84(2), 265–71. doi:10.1016/j.mimet.2010.12.009

[11] Cheng, H. D., Jiang, X. H., Sun, Y., & Wang, J. (2001). Color image segmentation: advances and prospects. Pattern Recognition, 34(12), 2259–2281. doi:10.1016/S0031-3203(00)00149-7

[12] Rodríguez-Pulido, F. J., Gómez-Robledo, L., Melgosa, M., Gordillo, B., González-Miret, M. L., & Heredia, F. J. (2012). Ripeness estimation of grape berries and seeds by image analysis. Computers and Electronics in Agriculture, 82, 128–133. doi:10.1016/j.compag.2012.01.004

[13] Whalley, J. L. (2013). Applications of image processing in viticulture: A review.

[14] Camera Calibration Toolbox For Matlab, http://www.vision.caltech.edu/bouguetj/calib_doc/ accessedMay 21 - Bouguet – 2007

[15] Z Zhang, "Flexible Camera Calibration by Viewing a Plane from Unknown Orientations," in ICCV, 1999, pp. 666–673.